Applied Mathematics & Information Sciences
An International Journal

http://dx.doi.org/10.18576/amis/200516

A Statistical Fractal Framework for Early Detection of Cardiac Abnormalities from ECG Signals

Fuad S. Al-Duais[1,*], *Galal Abdulqader Ahmed Alashaari*[1], *Yasser Mahmoud Aboelmaga*[2], *Ahmed I. Taloba*[3]

[1]Department of Mathematics, College of Science and Humanities in Al-Kharj, Prince Sattam Bin Abdulaziz University 11942 Al-Kharj, Saudi Arabia
[2]College of Engineering, University of Business and Technology, Jeddah, 23435, Saudi Arabia
[3]Department of Information System, Faculty of Computers and Information, Assiut University, Assiut, Egypt

Received: 30 Mar. 2026, Revised: 13 Jul. 2026, Accepted: 20 Jul. 2026
Published online: 1 Sep. 2026

Abstract: Electrocardiogram (ECG) signals exhibit nonlinear, nonstationary, and multiscale fluctuations that reflect the underlying dynamics of cardiac electrical activity. This study proposes a statistical fractal framework for the early detection of cardiac abnormalities based on the estimation and inferential analysis of multiscale complexity measures. Wavelet Packet Decomposition is used to obtain scale-specific energy distributions, while Detrended Fluctuation Analysis (DFA), Higuchi Fractal Dimension (HFD), correlation dimension, and multifractal spectrum width are employed to quantify temporal dependence, geometric complexity, attractor structure, and scaling heterogeneity, respectively. The statistical properties of these estimators are assessed using bootstrap confidence intervals and resampling-based hypothesis tests. Differences between normal and abnormal ECG recordings are evaluated in terms of effect sizes, confidence intervals, and multiplicity-adjusted significance levels. The extracted descriptors are subsequently combined into an Adaptive Cardiac Fractal Complexity Index (ACFCI), whose weights are estimated from the training data using regularized statistical learning. The discriminative ability of the index is examined through receiver operating characteristic analysis, cross-validation, sensitivity, specificity, and calibration measures. Normal ECG signals exhibit higher fractal organization, with DFA exponents ranging from 0.98 to 1.12, HFD values from 1.55 to 1.75, and multifractal spectrum widths from 0.55 to 0.90. Abnormal recordings show lower scaling consistency, with corresponding ranges of 0.72–0.92, 1.25–1.55, and 0.20–0.55. The estimated mean correlation dimension decreases from 3.42 ± 0.18 in normal recordings to 2.17 ± 0.23 in abnormal recordings, indicating a substantial reduction in dynamical complexity. The ACFCI ranges from 0.70 to 0.90 for normal ECG signals and from 0.20 to 0.65 for abnormal signals. When incorporated into a regularized logistic classification model, the proposed index achieves an estimated cross-validated accuracy of 97.0%. Its performance is also evaluated using confidence intervals for the area under the ROC curve and other clinically relevant classification measures. These findings provide statistical evidence that cardiac abnormalities are associated with a measurable breakdown of multiscale fractal organization. The proposed framework therefore offers an interpretable inferential approach for quantifying ECG complexity and detecting cardiac abnormalities.

Keywords: Good Health and Well-being (SDG 3); Cardiovascular Disease; Early Detection; Preventive Healthcare; Electrocardiogram (ECG); Cardiac Abnormality Detection; Statistical Fractal Analysis; Healthcare in Al-Kharj.

1 Introduction

Cardiovascular diseases (CVDs) remain public health problem and one of the most common causes of death and disability worldwide [1, 2]. Arrhythmia, myocardial infarction, heart failure and ischemic heart disease are disorders that affect millions of people every year and impose heavy clinical, social and economic burden on the healthcare system [3]. The early detection of these cardiac abnormalities is important to provide timely medical intervention, slow the progression of the disease, prevent serious complications and promote better patient outcomes [4]. The electrocardiogram (ECG) is among the different diagnostic tests that can be used and is one of the most commonly used and accurate methods to assess the heart's health [5, 6]. The ECG signals are non-invasive and cost-effective measures of the electrical activity of the

* Corresponding author e-mail: f.alduais@psau.edu.sa

heart, which are generated during each cardiac cycle and correspond to the changes in voltage caused by the depolarization and repolarization [7]. The recordings provide useful information on cardiac rhythm, conduction faults and cardiovascular function [8]. Because of its ease of use and diagnostic value, ECG monitoring is widely used in hospitals, I.C.U., ambulatory monitoring systems and wearable healthcare devices [9]. Recent developments in digital signal processing, machine learning and artificial intelligence have resulted in the rapid progress of automated ECG analysis systems that can interpret a greater amount of cardiac data more quickly [10, 11]. These smart programs can help clinicians make more accurate diagnoses, minimize observer variability, and monitor the patient continuously for early signs of cardiac diseases [12, 13].

Traditional methods of ECG interpretation focus mainly on the morphology and temporal features of the waveforms, such as the morphology of the P-wave, the duration of the QRS, the T-wave pattern, the variation of the RR interval, the deviation of the ST segment, the heart rate variability, and the amplitude [14]. While these features have been successful in the diagnosis of a variety of cardiovascular diseases and are important to clinical practice, they have been primarily employed to characterize the observed properties of the signal and offer information about processes are actually occurring in the body to create cardiac electrical activity [15]. The heart is in fact a complex, nonlinear dynamical system that is controlled by interplay between the autonomic nervous system, cardiac conduction pathways, neurohormone regulation and cardiovascular feedback mechanisms [16, 17]. These processes are interrelated and continually change to physiological and environmental stimuli, resulting in ECG signals with non-linear, nonstationary and dynamically changing behavior [18, 19]. As a result, conventional linear and morphology-based descriptors are unsuitable to properly reflect subtle pathological changes [20]. Recent research indicates that the information that leads to diagnostic judgments is not just contained in the prominent structure of the ECG signal, but rather in the invisible factors of signal complexity, self-similarity and dynamic organization [21, 22]. These deeper dynamical properties, which are not captured by traditional statistical and time domain measures, can only be detected for abnormalities earlier in their development and complex cardiac dysfunctions [23]. Thus, sophisticated analysis tools that can capture the dynamic, multiscale complexity and hidden temporal interaction between variables are needed to unlock the underlying physiology and facilitate more accurate, robust, and interpretable cardiovascular disease diagnosis [24].

Existing studies, however, vary significantly in how they deal with the fractal properties, including just fractal dimension estimation to multifractal analysis and hybrid deep-learning frameworks. Sabrine and Taoufik [25] gave an ample knowledge about fractal dimensions and they showed that ECG signals are fractal also and discussed cardiac disease classification. With their work they laid the theoretical framework that ECG signals have irregular and fractal properties which can be measured by fractal dimensions. The framework is thus restricted in its ability to characterize the heterogeneous complexity patterns for each type of cardiac abnormality. Riccio et al. [26] proposed a new approach to representing PCG signals with PIFS and DCNNs. They used self-similarity-based representations to generate two-dimensional fractal images from one-dimensional cardiac signals and showed that this kind of representation has the potential of classification. The main drawback in the suggested method was its focus on signal representation instead of quantitative fractal characterization; thus, fractal images were prepared to be classified by a DL algorithm, but the images were not explicitly interpreted as physiological aspects of cardiac complexity or dynamics.

Berrahou et al. [27] presented arrhythmia classification and added auxiliary feature Higuchi Fractal Dimension. However, the fractal analysis was not a central element of the whole. It did not use multifractal structures, long-range correlations or integrated complexity representations, and a single fractal measure was used. Accordingly, the potential of fractal geometry for characterizing pathological cardiac dynamics has been under-explored. Pekcan and Arsan [28] proposed a geometry-based approach that used phase-space trajectory and box-counting fractal dimensions for ECG signals. But only global fractal dimension and other global parameters were analyzed and multiscale fluctuations, multifractal spectra, and feature integration strategies that could enhance diagnostic discrimination were not included.

Azizi [29] showed the importance of multifractal analysis in fetal ECG studies. The study demonstrated that the tools of power spectral analysis, multifractal spectra, and Higuchi fractal dimensions can be used to characterize the complexity of signals and distinguish the patterns of physiology. Furthermore, the thresholds and clinical interpretation of the extracted fractal measures were not completely specified. Dorostghol et al. [30] explored prediction of sudden cardiac death by using the Detrended Fluctuation Analysis of HRV signals which is a multifractal approach. They showed that MF-DFA is able to distinguish SCE and CHF cases using EMD and Teager energy operators, which are multifractal features. However, was limited to HRV-derived features and SVM classification, and therefore only applicable to direct analysis of the ECG waveform complexity and a wider range of cardiac abnormalities.

Babini et al. [31] examined complexity relationships between EEG and heart rate variability, as well as during olfactory stimulation, using fractal theory and entropy measures. They showed that the patterns of physiological complexity are highly correlated among organ systems. The study confirmed the biological relevance of fractal complexity as a physiological marker, but was not

undertaken for the purpose of diagnosis of disease and so did not consider the formation of predictive classification systems. Alohali et al. [32] delved into DL and cloud-IoT technologies in myocardial energy autophagy analysis. The authors proposed that, although fractal theory was not directly used in the analytical process, fractal inspired optimization can be used to improve the performance of deep learning models. The study showed the increasing awareness of applying fractal principles to AI, but it did not explicitly include fractal descriptors, scaling analysis or quantification of the complexity, which restrict the application to fractal cardiac diagnosis. Pander [33] suggested an advanced algorithm for detecting AF by employing wavelet transforms, Hilbert based decompositions, entropy measures, and ML classifiers. However, the method was essentially based on statistical and spectral features. Thus, the analysis of self-similarity, scaling property, and multifractal organization of ECG signals were not explicitly modeled. To perform ECG denoising, Zhang et al. [34] used a regularization-dimension filter based on fractal features. But the processing was focused mainly on preprocessing and not on the characterization of disease and used no fractal information to assess the disease complexity and classification. In conclusion, the literature establishes fractal analysis as a powerful tool to describe the complexity of the physiological system and dynamics of the heart. While this is extremely promising, there are some obvious weaknesses.

The fractal dimension-based approaches have been proven to quantify the irregularity and complexity of the signals, but most of the researches have been based on a single fractal dimension such as Higuchi, Katz, Box-counting or similar, which provides only partial representation of the underlying cardiac dynamics [25, 29]. In recent ECG classification tools, fractal measures have been introduced as auxiliary features in DL architectures, and high diagnostic performance have been obtained in the detection of arrhythmias, however, the multiscale scaling behavior and the nonlinear complexity of ECG signals are not fully investigated [26, 27]. Moreover, both phase-space and nonlinear dynamical approaches have revealed that fractal geometry and attractor structures have potential applications as a source of information for discriminating normal and pathological cardiac states, but most of these studies have considered only individual geometric features, and they do not simultaneously model long-range temporal correlation, waveform complexity, and multifractal organization within a single framework [28, 30]. Consequently, there is a lack of a comprehensive research framework that describes the multiscale dynamics, long-range correlations, complexity of the waveforms, and multifractal behavior of the ECG signals simultaneously. To overcome this, the present work proposes a combined wavelet packet decomposition, detrended fluctuation analysis, Higuchi fractal dimension and multifractal spectrum analysis-based fractal DL framework to obtain complementary complexity descriptors from ECG signals. These descriptors are then fused using a novel ACFCI to obtain a comprehensive fractal representation which is processed with a lightweight 1D-CNN for the purpose of robust and automatic cardiac abnormality classification.

Key Contributions

1. A unified fractal analysis framework integrating WPD, DFA, HFD, and Multifractal Spectrum Analysis for multiscale characterization of ECG dynamics.
2. A novel ACFCI that jointly models long-range correlations, local waveform complexity, and multifractal scaling behavior within a single complexity descriptor.
3. A fractal feature representation that preserves hierarchical cardiac scaling information and provides a more comprehensive description of ECG dynamics than individual fractal measures.
4. A lightweight 1D-CNN framework designed to learn discriminative relationships among fractal descriptors for automated cardiac abnormality detection.
5. A comprehensive evaluation demonstrating the effectiveness of integrated fractal dynamics for distinguishing normal and pathological cardiac conditions.

2 Fractal-Geometric and Multiscale Complexity Learning Framework for Cardiac Abnormality Detection

This section introduces the proposed Fractal geometric and multiscale deep learning approach for detection of cardiac abnormalities in ECG signals. The system combines wavelet packet decomposition, differential geometric modeling, phase-space reconstruction, fractal scaling analysis, multifractal spectrum characterization, and the proposed ACFCI to comprehensively address various aspects of cardiac dynamics. The extracted fractal descriptors are then modeled jointly by geometric deformation, nonlinear evolution, long-range correlations and multiscale complexity, and then a unified feature representation is learned using a lightweight 1D-CNN for robust cardiac state classification. It is clearly depicted in Fig. 1.

2.1 ECG Acquisition and Preprocessing

In this study, ECG signals are drawn from the PTB-XL database, which features 12-lead ECG recordings from 18,869 patients with 21,799 clinically annotated signals [35]. The duration of each recording is 10s and it consists of normal and pathological cardiac activities. Let the acquired ECG signal be represented as eqn. (1).

$$x(t) = \{x_1, x_2, \ldots, x_N\} \tag{1}$$

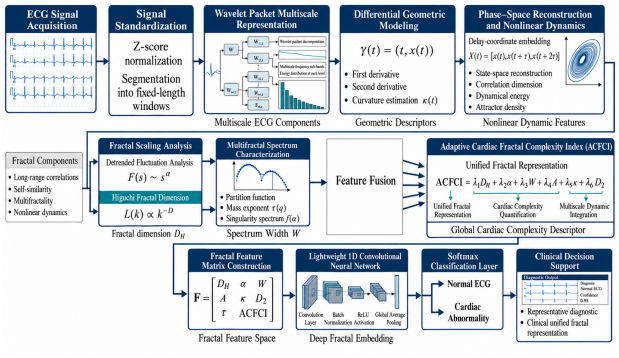

Fig. 1: Overall workflow for Cardiac Abnormality Detection

where $x(t)$ is the amplitude of the electrocardiogram at time t, and N is the total number of samples.
In order to achieve scale invariance and enable fractal analysis, each electrocardiogram recording is normalized using the z-score normalization technique as given in eqn. (2).

$$x_{\text{norm}}(t) = \frac{x(t) - \mu}{\sigma} \tag{2}$$

where $x(t)$ is the original electrocardiogram, μ is the mean of the signal, and σ is the standard deviation of the signal. The normalized signal is then divided into segments of predetermined lengths in order to capture the cardiac dynamics at different scales. The i^{th} segment of the ECG is represented by eqn. (3).

$$S_i = \{x_{norm}(n)\}_{n=(i-1)L+1}^{iL} \tag{3}$$

Where S_i is the i^{th} segment of the ECG, L denotes length of the segment, and i denotes segment index.
These segments of ECG signals ensure standardized representation of signals to undergo further multiscale decomposition, fractal geometry processing, and nonlinearity analysis of cardiac complexity. This process helps in establishing mathematical fundamentals required for understanding scaling features and fractality in the dynamics of cardiac electricity.

2.2 Wavelet Packet Decomposition-Based Multiscale Representation

To study the multiscale dynamics of heart activities, the processed ECG signal $x_n(t)$ was decomposed through Wavelet Packet Decomposition (WPD). In contrast to traditional wavelet transform, where decomposition is done iteratively on the approximation coefficient, WPD involves complete binary tree decomposition of both approximation and detail signals.

In the case of decomposition level j, the ECG signal can be expressed as in eqn. (4).

$$W_{j,k}(t) = \int_{-\infty}^{\infty} x_{\text{norm}}(t)\, \psi_{j,k}(t)\, dt \tag{4}$$

where $W_{j,k}$ denotes the wavelet packet decomposition (WPD) coefficient, $x_{\text{norm}}(t)$ is the normalized ECG signal, and $\psi_{j,k}(t)$ is the wavelet packet basis function. Here, j denotes the decomposition level, and k denotes the node index within the wavelet packet tree.

$$V_{j,k}(t) = \sum_n g(n) V_{j-1,k}(2t - n) \tag{5}$$

Where $h(n)$and $g(n)$ represent low-pass and high-pass filter coefficients, respectively,
The decomposition process results in a set of sub-bands that are localized in frequency. It is given in eqn. (6).

$$\mathscr{W} = \{W_{j,1}, W_{j,2}, \ldots, W_{j,M}\} \tag{6}$$

Where $M = 2^j$ represents the total number of sub-bands at level j.
The energy distribution of each sub-band was computed as given in eqn. (7).

$$E_k = \sum_t |W_{j,k}(t)|^2 \tag{7}$$

This helps identify the most informative scales related to cardiac dynamics. They keep the sub-bands that show significant energy concentration and structural variability for later fractal and multifractal analysis [36]. So, the WPD stage changes the normalized ECG signal into a multiscale representation, like in eqn. (1). It preserves both low-frequency cardiac trends and high-frequency fluctuations, which are crucial for understanding the ECG signal's hierarchical fractal organization.

2.3 Differential Geometric Modeling of ECG Dynamics

After WPD, the normalized ECG signal is represented as a differentiable geometric trajectory in a Euclidean manifold, which allows the representation of cardiac electrical activity as a measurable curve of continuous geometric trajectories [37]. Consider the ECG signal as a scalar function of time $x(t)$ and the ECG trajectory in the phase plane as given in eqn. (8).

$$\boldsymbol{\gamma}(t) = \big(t, x(t)\big) \tag{8}$$

where $\boldsymbol{\gamma}(t)$ denotes the ECG trajectory in the two-dimensional Euclidean space, t is the temporal coordinate, and $x(t)$ denotes the ECG amplitude. The tangent vector field describes the instantaneous geometric changes of the trajectory as represented in eqn. (9).

$$\mathbf{T}(t) = \frac{d\boldsymbol{\gamma}(t)}{dt} = \left(1, \frac{dx(t)}{dt}\right) \tag{9}$$

where $\mathbf{T}(t)$ is the tangent vector to the ECG curve at time t, and $\frac{dx(t)}{dt}$ is the instantaneous rate of change of the ECG amplitude.
The length of the tangent vector is defined as eqn. (10).

$$\|\mathrm{T}(t)\| = \sqrt{1 + \left(\frac{dx(t)}{dt}\right)^2} \tag{10}$$

where $\|\mathrm{T}(t)\|$ is a measure of the instantaneous geometric deformation of the ECG trajectory. The normalized tangent field is given as eqn. (11).

$$\widehat{\mathbf{T}}(t) = \frac{\mathbf{T}(t)}{\|\mathbf{T}(t)\|} \tag{11}$$

where $\widehat{\mathbf{T}}(t)$ is the unit tangent vector representing the local orientation of the ECG trajectory and, consequently, the local direction of cardiac electrical propagation.
The first-order temporal derivative of the ECG signal is defined as

$$v(t) = \frac{dx(t)}{dt}, \tag{12}$$

where $v(t)$ denotes the instantaneous slope of the ECG signal and represents the local rate of change of its amplitude with respect to time.
The mean absolute slope of the ECG signal is defined as

$$\bar{v} = \frac{1}{N}\sum_{i=1}^{N} |v(t_i)| = \frac{1}{N}\sum_{i=1}^{N} \left| \frac{dx(t)}{dt}\bigg|_{t=t_i} \right|, \tag{13}$$

where N is the number of ECG samples and $\bar{v}$ measures the average magnitude of the temporal amplitude variation. It therefore provides a summary of the overall rate of change of the ECG waveform.
The second-order temporal derivative of the ECG signal is defined as

$$a(t) = \frac{d^2x(t)}{dt^2}, \tag{14}$$

where $a(t)$ represents the instantaneous rate of change of the ECG slope. Large magnitudes of $a(t)$ indicate rapid changes in waveform morphology.
The accumulated squared second-derivative measure over the recording duration T is defined as

$$E_a = \int_0^T \left(\frac{d^2x(t)}{dt^2}\right)^2 dt = \int_0^T a^2(t)\,dt, \tag{15}$$

where E_a denotes the acceleration energy of the ECG signal. It quantifies the cumulative magnitude of rapid changes in the waveform slope over the interval $[0,T]$.
Local curvature of the ECG trajectory is given in eqn. (16).

$$\kappa(t) = \frac{\left|\frac{d^2x(t)}{dt^2}\right|}{\left[1 + \left(\frac{dx(t)}{dt}\right)^2\right]^{3/2}} \tag{16}$$

where $\kappa(t)$ denotes the curvature of the ECG trajectory and measures the instantaneous geometric bending of the ECG waveform at time t.
The mean curvature is calculated as given in eqn. (17).

$$\bar{\kappa} = \frac{1}{T}\int_0^T \kappa(t)\,dt \tag{17}$$

where $\bar{\kappa}$ denotes the mean curvature, representing the average geometric bending of the ECG trajectory over the time interval $[0,T]$.
The variance of the curvature is given in Equation (18).

$$\sigma_\kappa^2 = \frac{1}{T}\int_0^T (\kappa(t) - \bar{\kappa})^2\,dt \tag{18}$$

where σ_κ^2 denotes the curvature variance and quantifies fluctuations in the geometric bending of the ECG trajectory. Larger values indicate greater waveform irregularity.
The length of the ECG curve is given by the eqn. (19).

$$L = \int_0^T \sqrt{1 + \left(\frac{dx(t)}{dt}\right)^2}\,dt \tag{19}$$

where L denotes the total geometric arc length of the ECG trajectory $\boldsymbol{\gamma}(t) = (t, x(t))$ over the time interval $[0,T]$. The normalized arc-length complexity is given by eqn. (20).

$$L_\mathrm{n} = \frac{L}{T} \tag{20}$$

where L_n denotes the time-normalized geometric path length of the ECG trajectory and provides a measure of its average geometric complexity per unit time.
The curvature energy functional is given in eqn. (21).

$$E_\kappa = \int_0^T \kappa^2(t)\,dt \tag{21}$$

where E_κ denotes the total bending energy and quantifies the overall curvature of the ECG trajectory over the time interval $[0,T]$. Larger values indicate stronger or more frequent geometric bending.
At the end, all the geometric descriptors get mixed into one feature representation as given in eqn. (22).

$$\mathbf{G} = [\bar{v}, E_a, \bar{\kappa}, \sigma_\kappa, L_\mathrm{n}, E_\kappa]^\mathsf{T} \tag{22}$$

where $\mathbf{G}$ is the geometric feature vector comprising the mean slope $\bar{v}$, acceleration energy E_a, mean curvature $\bar{\kappa}$, curvature standard deviation σ_κ, normalized arc length L_n, and total bending energy E_κ of the ECG trajectory.

2.4 Phase-Space Reconstruction and Nonlinear Dynamic Analysis

In addition to being represented as a one-dimensional temporal signal, the ECG signal is modeled as the

observable projection of an underlying nonlinear dynamical system (NLS) modeling the cardiac electrical activity. The ECG is embedded in phase space to reveal states and pathways that were not obvious in the original data by applying the theory of delay-coordinate embedding. The theory of delay-coordinate embedding is used to reconstruct the ECG as a multidimensional dynamical trajectory to uncover hidden states and pathways, as well as long range dependencies and nonlinear interactions.
The reconstructed state space representation of the ECG signal is given by eqn. (23).

$$\mathbf{X}(t) = \begin{bmatrix} x(t) \\ x(t+\tau) \\ x(t+2\tau) \\ \vdots \\ x\big(t+(m-1)\tau\big) \end{bmatrix} \in \mathbb{R}^m \tag{23}$$

where $\mathbf{X}(t)$ is the reconstructed cardiac state vector obtained from the ECG signal, m is the embedding dimension, τ is the time delay, and $x(t)$ is the ECG amplitude at time t. The embedding dimension m determines the dimensionality of the reconstructed phase space.
The dynamics of the heart is expressed as a non-linear, discrete flow map is given in eqn. (24).

$$\mathbf{X}(t+\Delta t) = F\big(\mathbf{X}(t)\big) \tag{24}$$

where $F(\cdot)$ denotes the unknown nonlinear cardiac-state evolution operator, and Δt is the sampling interval.
This formulation makes it possible to interpret ECG analysis as a state transition dynamical system and hence geometrically describe the cardiac evolution.
To measure local deformation and stability of the reconstructed attractor, the Jacobian matrix of the flow is given by eqn. (25).

$$J(t) = \frac{\partial F(X)}{\partial X}|_{X=X(t)} \tag{25}$$

Where, $\mathrm{J}(t) \in \mathbb{R}^{m\times m}$ is the local phase space deformation. The spectrum of eigenvalues is calculated from eqn. (26).

$$\det(\mathbf{J} - \lambda \mathbf{I}) = 0 \tag{26}$$

where λ_i are the eigenvalues of the Jacobian matrix $\mathbf{J}$ and characterize the local growth or decay of perturbations to the cardiac trajectory. The matrix $\mathbf{I}$ is the identity matrix.
The pairwise distance metric is defined as eqn. (27).

$$d_{ij} = \big\|\mathbf{X}(t_i) - \mathbf{X}(t_j)\big\|_2 = \sqrt{\sum_{k=0}^{m-1} \big[x(t_i+k\tau) - x(t_j+k\tau)\big]^2} \tag{27}$$

where d_{ij} denotes the Euclidean distance between the cardiac states $\mathbf{X}(t_i)$ and $\mathbf{X}(t_j)$. It quantifies their separation in the reconstructed phase space and can be used to assess the divergence of nearby trajectories.
A density function is used to quantify the statistical occupation of phase space, and it is given in eqn. (28).

$$\rho(\mathbf{X}) = \lim_{\varepsilon\to 0} \frac{N_\varepsilon(\mathbf{X})}{NV_\varepsilon} \tag{28}$$

where $N_\varepsilon(\mathbf{X})$ is the number of reconstructed trajectory points within an ε-neighborhood of $\mathbf{X}$, N is the total number of trajectory points, and V_ε is the corresponding phase-space volume. The density $\rho(\mathbf{X})$ characterizes the local clustering of cardiac trajectories in the reconstructed phase space.
The correlation integral is used to calculate the fractal structure in the nonlinear dynamics as follows in eqn. (29).

$$C(r) = \lim_{N\to\infty} \frac{2}{N(N-1)} \sum_{i<j} H(r - d_{ij}) \tag{29}$$

Where $H(\cdot)$ denotes the Heaviside step function, r is the phase space radius, and d_{ij} denotes the inter-state distance.
The scaling law of the system is given in eqn. (30).

$$C(r) \propto r^{D_2} \tag{30}$$

The correlation dimension is obtained as eqn. (31).

$$D_2 = \frac{d\log C(r)}{d\log r} \tag{31}$$

Where fractal dimension, D_2 cardiac attractor quantitatively represents the complexity of the nonlinear cardiac geometry.
A Lyapunov-type divergence formulation is used for sensitivity to initial conditions. It is given in eqn. (32).

$$\|\delta\mathbf{X}(t)\|_2 \approx \|\delta\mathbf{X}(0)\|_2 e^{\lambda t} \tag{32}$$

where $\delta\mathbf{X}(t)$ denotes the separation between two initially neighboring trajectories at time t, and λ is the divergence exponent. A positive value of λ indicates exponential divergence and local dynamical instability, whereas a negative value indicates convergence.
The global energy of the reconstructed attractor is given by eqn. (33).

$$E_{\text{dyn}} = \int_0^T \left\| \frac{d\mathbf{X}(t)}{dt} \right\|_2^2 dt \tag{33}$$

where E_{dyn} denotes the total dynamical activity of the reconstructed cardiac-state trajectory over the interval $[0,T]$. It quantifies the accumulated squared speed of the trajectory through the reconstructed phase space, and $\Gamma = \{\mathbf{X}(t) : 0 \le t \le T\}$ denotes the corresponding trajectory on the reconstructed attractor.
Finally, all the above nonlinear dynamical descriptors are summarized in a common feature representation as given

in eqn. (34).

$$\mathbf{P} = \begin{bmatrix} D_2 \\ \lambda \\ \rho \\ E_{\text{dyn}} \\ \langle d_{ij} \rangle \end{bmatrix} \tag{34}$$

where $\mathbf{P}$ is the nonlinear dynamical feature vector comprising the correlation dimension D_2, Lyapunov-type divergence exponent λ, attractor-density measure ρ, dynamical energy E_{dyn}, and mean pairwise distance $\langle d_{ij} \rangle$ in the reconstructed phase space.

2.5 Fractal Scaling and Complexity Analysis

The ECG signal is modeled as a non-stationary self-affine fractal process with multiscale scaling properties, after phase-space reconstruction and geometric transformation. Detrended Fluctuation Analysis (DFA) and Higuchi Fractal Dimension (HFD) are formulated as coupled scaling operators on the reconstructed cardiac trajectory to quantify in a unified mathematical framework the long-range dependence and waveform complexity.
The ECG process is defined as given in eqn. (1). This is the same integrated profile but done over a cumulative period given by eqn. (35).

$$Y(k) = \sum_{i=1}^{k} (x_i - \mu_x), \qquad k = 1, \ldots, N \tag{35}$$

where x_i is the ECG amplitude at the i-th discrete-time sample, N is the total number of samples, μ_x is the mean ECG amplitude, and $Y(k)$ is the cumulative mean-centered profile used for fractal scaling analysis.
The integrated signal is broken down into different parts according to scale, and it is represented in eqn. (36).

$$Y_v(j) = Y\big((v-1)s + j\big), \qquad v = 1, \ldots, N_s, \quad j = 1, \ldots, s \tag{36}$$

where s is the window length (scale), $N_s = \lfloor N/s \rfloor$ is the number of nonoverlapping segments, v is the segment index, and j is the local sample index within each segment.
The local trend is estimated in each segment using polynomial regression and it is represented in eqn. (37).

$$P_v(j) = arg\,min_P \sum_{j=1}^{s} \left(Y_v(j) - P(j)\right)^2 \tag{37}$$

where $P_v(j)$ is the local polynomial trend in the v^{th} segment.
The detrended fluctuation field is given by eqn. (38).

$$\varepsilon_v(j) = Y_v(j) - P_v(j) \tag{38}$$

In the above equations $\varepsilon_v(j)$ represents the detrending fluctuation, namely the fluctuation that is obtained by subtracting the local trend from the original random process.

The local variation of fluctuations at scale s is given by eqn. (39).

$$F^2(v,s) = \frac{1}{s} \sum_{j=1}^{s} \varepsilon_v^2(j) \tag{39}$$

where $F^2(v,s)$ means the fluctuation variance of the v^{th} segment at scale s.
The fluctuation function for the global is given by eqn. (40).

$$F(s) = \sqrt{\frac{1}{N_s} \sum_{v=1}^{N_s} F^2(v,s)} \tag{40}$$

Where $F(s)$ is the global magnitude of fluctuation.
The ECG shows self-affine fractal scaling, which is controlled by eqn. (41).

$$F(s) \propto s^{\alpha} \tag{41}$$

where α is the detrended fluctuation analysis (DFA) scaling exponent, estimated as the slope of $\log F(s)$ versus $\log s$, and characterizes the temporal correlation structure of the ECG signal.
Taking logarithmic transformation as eqn. (42).

$$\log F(s) = \alpha \log s + C \tag{42}$$

where α is the DFA scaling exponent, obtained as the slope of the linear relationship between $\log F(s)$ and $\log s$, and C is a scale-independent intercept.
The DFA exponent is the result of a differential scaling operator as eqn. (43).

$$\alpha = \frac{d \log F(s)}{d \log s} \tag{43}$$

where α is the local slope of the fluctuation function on a log–log scale and quantifies the scale-dependent temporal correlation structure of the ECG signal. Values of $\alpha > 0.5$ generally indicate persistent correlations, whereas $\alpha < 0.5$ indicates antipersistent correlations.
Higuchi fractal construction defined by embedding, to characterize geometric complexity of waveform as given in eqn. (44).

$$X_k^m = \{x(m), x(m+k), x(m+2k), \ldots\} \tag{44}$$

Where k represents the scale interval, and the m represents the starting point in the construction of Higuchi curves.
The length of the curve at scale $k$is calculated to be eqn. (45).

$$L_m(k) = \frac{N-1}{k^2} \sum_{i=1}^{\lfloor \frac{N-m}{k} \rfloor} | \, x(m+ik) - x(m+(i-1)k) \, | \tag{45}$$

where $L_m(k)$ represents the curve length associated with scale k and offset m.

Overall average for all offsets is given in eqn. (46).

$$L(k) = \frac{1}{k}\sum_{m=1}^{k} L_m(k) \tag{46}$$

Where $L(k)$ denotes the average curve length over all offsets.
The Higuchi fractal scaling law follows as given in eqn. (47).

$$L(k) \propto k^{-D_H} \tag{47}$$

where D_H denotes Higuchi fractal dimension which represents the roughness of the ECG wave form.
Taking logarithm as given in eqn. (48).

$$\log L(k) = -D_H \log k + C \tag{48}$$

Where slope of the log-log relationship gives the fractal dimension D_H.
The Higuchi fractal dimension is given by eqn. (49).

$$D_H = -\frac{d\log L(k)}{d\log k} \tag{49}$$

where D_H calculates the geometric complexity on several scales.
The coupled fractal consistency over the scaling regimes is stipulated as eqn. (50).

$$\frac{d\alpha}{ds}\frac{dD_{\mathrm{H}}}{ds} \neq 0 \tag{50}$$

Where multiscale fractal adaptation in cardiac dynamics is active as evidenced by nonzero coupled derivatives, which suggests that cardiac dynamics at multiple scales are active, whereas eqn. (51).

$$\frac{d\alpha}{ds} = 0, \qquad \frac{dD_{\mathrm{H}}}{ds} = 0 \tag{51}$$

Where it indicates loss of physiological rigidity and pathological ECG behavior, fractal adaptability.
Lastly, the fractal descriptors of scaling are combined in a short complexity vector. It is given in eqn. (52).

$$\mathbf{F}_{\mathrm{scaling}} = \begin{bmatrix} \alpha \\ D_{\mathrm{H}} \\ \dfrac{d\alpha}{ds} \\ \dfrac{dD_{\mathrm{H}}}{ds} \end{bmatrix} \tag{52}$$

where $\mathbf{F}_{\mathrm{scaling}}$ is the fractal-scaling feature vector comprising the DFA scaling exponent α, Hausdorff dimension D_{H}, and their scale-dependent gradients. This vector is subsequently used in the multifractal analysis and the construction of the ACFCI.

2.6 Multifractal Spectrum Characterization

After the multiscale decomposition and nonlinear dynamical reconstruction of the ECG, it shows a spatially and temporally varying scaling behavior which cannot be described by a single fractal exponent. To overcome this, the ECG signal is represented as a multifractal measure, such that the scaling exponents in different regions of the signal are different. This allows the characterization of heterogeneous cardiac dynamics in normal and pathological states.

Let the ECG signal be defined as in Equation (1). To construct a scale-dependent measure, the signal is partitioned into intervals of size ε, and a normalized probability measure is defined as in Equation (53).

$$p_i(\varepsilon) = \frac{\sum_{k\in B_i(\varepsilon)} |x_k|}{\sum_{k=1}^{N} |x_k|} \tag{53}$$

Where $p_i(\varepsilon)$ denotes the probability mass in the i^{th} box, $B_i(\varepsilon)$ indicates samples in the i^{th} partition, and ε is the scale parameter. This makes the ECG a scale dependent probability field, so that it can be analyzed using multifractal analysis. The generalized partition function is given by eqn. (54).

$$Z(q,\varepsilon) = \sum_{i=1}^{N(\varepsilon)} [p_i(\varepsilon)]^q \tag{54}$$

Where $Z(q,\varepsilon)$ indicates a generalized partition function, q is the moment order, and $N(\varepsilon)$ is the number of partitions at scale ε. This formulation is for amplification of large fluctuations for $q > 0$, small fluctuations for $q < 0$.
The ECG shows power law scaling of the form as eqn. (55).

$$Z(q,\varepsilon) \propto \varepsilon^{\tau(q)} \tag{55}$$

where $Z(q,\varepsilon)$ is the partition function of statistical order q at observation scale ε, and $\tau(q)$ is the mass-scaling exponent characterizing the multifractal scaling behavior.
Taking the logarithm of Equation (55) yields

$$\log Z(q,\varepsilon) = \tau(q)\log\varepsilon + C, \tag{56}$$

where C is a scale-independent constant and $\tau(q)$ is the mass-scaling function of the ECG signal. The mass exponent is defined as

$$\tau(q) = \lim_{\varepsilon\to 0} \frac{\log Z(q,\varepsilon)}{\log\varepsilon}. \tag{57}$$

Here, $\tau(q)$ denotes the asymptotic scaling exponent obtained from the partition function. Equivalently, its local differential form is given by

$$\tau(q) = \frac{d\log Z(q,\varepsilon)}{d\log\varepsilon}, \tag{58}$$

where the derivative represents the logarithmic rate of change of the partition function with respect to the observation scale.
The singularity-strength function is computed as

$$\alpha(q) = \frac{d\tau(q)}{dq}, \tag{59}$$

where $\alpha(q)$ is the local Hölder exponent, also called the singularity strength, associated with the statistical order q. The multifractal spectrum is then obtained through the Legendre transform:

$$f\big(\alpha(q)\big) = q\alpha(q) - \tau(q). \tag{60}$$

Here, $f(\alpha)$ is the multifractal spectrum, and α is the singularity strength. The Legendre transform maps the global scaling properties described by $\tau(q)$ to a geometric spectrum describing the distribution of local singularities. The Legendre-transform relation implies

$$\frac{df(\alpha)}{d\alpha} = q, \tag{61}$$

where q controls the relative contributions of different singularities. Positive values of q emphasize regions with larger measure, whereas negative values emphasize regions with smaller measure. A nonlinear mass-scaling function satisfies

$$\frac{d^2\tau(q)}{dq^2} \neq 0. \tag{62}$$

A nonzero second derivative indicates that $\tau(q)$ is nonlinear in q, which is a characteristic of multifractal scaling. In contrast, a linear $\tau(q)$ is associated with monofractal scaling. In empirical applications, multifractality should be established over a validated scaling range and supported by appropriate statistical testing.
Several descriptors can be derived from the estimated multifractal spectrum. Its width is defined as

$$W = \alpha_{\max} - \alpha_{\min}, \tag{63}$$

where $\alpha_{\min}$ and $\alpha_{\max}$ are the minimum and maximum singularity strengths, respectively. The spectrum width W describes the range of local scaling behavior; a larger value generally indicates greater multifractal heterogeneity.
The dominant singularity strength, corresponding to the peak of the multifractal spectrum, is

$$\alpha_0 = \arg\max_{\alpha} f(\alpha), \tag{64}$$

where α_0 is the singularity strength at which $f(\alpha)$ reaches its maximum.
The spectral asymmetry index is defined as

$$A = \frac{(\alpha_0 - \alpha_{\min}) - (\alpha_{\max} - \alpha_0)}{\alpha_{\max} - \alpha_{\min}}. \tag{65}$$

Here, A quantifies the asymmetry of the multifractal spectrum. A value of $A = 0$ indicates a symmetric spectrum, whereas the sign and magnitude of A describe the direction and degree of asymmetry under this convention.
The area under the multifractal spectrum is defined as

$$E_{\mathrm{MF}} = \int_{\alpha_{\min}}^{\alpha_{\max}} f(\alpha)\, d\alpha, \tag{66}$$

where E_{MF} summarizes the total area of the estimated multifractal spectrum over the observed range of singularity strengths.
Finally, the multifractal descriptor vector for the ECG signal is constructed as

$$\mathbf{M} = \begin{bmatrix} W \\ \alpha_0 \\ A \\ E_{\mathrm{MF}} \\ \boldsymbol{\tau} \end{bmatrix}, \qquad \boldsymbol{\tau} = \big[\tau(q_1)\ \tau(q_2)\ \cdots\ \tau(q_Q)\big]^{\mathsf{T}}, \tag{67}$$

where $\mathbf{M}$ is the multifractal descriptor vector and $\boldsymbol{\tau}$ contains the mass exponents evaluated at the selected statistical orders $q_1, q_2, \ldots, q_Q$.

2.7 Adaptive Cardiac Fractal Complexity Index (ACFCI)

After performing multiscale decomposition, nonlinear dynamical reconstruction, fractal scaling analysis, and multifractal spectrum characterization, ECG is described by a collection of heterogeneous descriptors related to the properties of its waveform, long-range correlations, geometric deformation and scaling variability. However, using these descriptors alone do not capture the coupled nature of cardiac complexity. In order to overcome this limitation, this study proposes a new single-scalar metric of cardiac dynamics, named the unified Adaptive Cardiac Fractal Complexity Index (ACFCI) that combines fractal, multifractal and geometric invariants together. Assume the feature set extracted is given by eqn. (68).

$$\mathscr{F} = \begin{bmatrix} \mathrm{FD_H} \\ \alpha \\ W \\ A \\ \bar{\kappa} \end{bmatrix}, \tag{68}$$

where $\mathrm{FD_H}$ denotes the Higuchi fractal dimension, α is the DFA scaling exponent, W is the multifractal spectrum width, A is the spectral asymmetry index, and $\bar{\kappa}$ is the mean curvature of the ECG trajectory.
Each feature is standardized as

$$\widetilde{f}_i = \frac{f_i - \mu_{f_i}}{\sigma_{f_i}}, \qquad i = 1, \ldots, 5, \tag{69}$$

where μ_{f_i} and σ_{f_i} are, respectively, the mean and standard deviation of feature f_i, estimated from the training data. The resulting normalized feature vector is

$$\widetilde{\mathscr{F}} = \begin{bmatrix} \widetilde{\mathrm{FD}}_{\mathrm{H}} \\ \widetilde{\alpha} \\ \widetilde{W} \\ \widetilde{A} \\ \widetilde{\bar{\kappa}} \end{bmatrix}. \tag{70}$$

Here, $\widetilde{\mathscr{F}}$ denotes the standardized fractal–geometric feature vector.

The ACFCI is defined as a projection of the normalized feature space onto a scalar complexity index:

$$\mathrm{ACFCI} = \Phi\left(\widetilde{\mathscr{F}}\right), \tag{71}$$

where $\Phi(\cdot)$ is a coupling operator that integrates the multiscale cardiac descriptors.

A weighted fusion formulation of the ACFCI is

$$\mathrm{ACFCI} = \lambda_1 \widetilde{\mathrm{FD}}_{\mathrm{H}} + \lambda_2 \widetilde{\alpha} + \lambda_3 \widetilde{W} + \lambda_4 \widetilde{A} + \lambda_5 \widetilde{\bar{\kappa}}, \tag{72}$$

where λ_i is the adaptive contribution weight associated with the i-th descriptor. The weights satisfy

$$\sum_{i=1}^{5} \lambda_i = 1, \qquad \lambda_i \geq 0. \tag{73}$$

These constraints make the ACFCI a convex combination of the normalized features.

The adaptive weights may be calculated using a softmax coupling function:

$$\lambda_i = \frac{\exp\left(\beta \widetilde{f}_i\right)}{\sum_{j=1}^{5} \exp\left(\beta \widetilde{f}_j\right)}, \qquad i = 1, \ldots, 5, \tag{74}$$

where β is a sensitivity parameter. When $\beta = 0$, all features receive equal weights. Increasing positive values of β assign greater weight to features with larger standardized values.

Alternatively, the fusion weights may be learned from N training observations by minimizing the regularized objective

$$\mathscr{J}(\boldsymbol{\lambda}) = \frac{1}{2N} \sum_{n=1}^{N} \left[y_n - \boldsymbol{\lambda}^{\mathsf{T}} \widetilde{\mathscr{F}}_n \right]^2 + \frac{\gamma}{2} \|\boldsymbol{\lambda}\|_2^2, \tag{75}$$

where y_n is the reference outcome or target complexity score for the n-th observation, $\boldsymbol{\lambda}$ is the weight vector, and $\gamma \geq 0$ is a regularization parameter used to control model complexity and reduce overfitting.

The stationary condition for the unconstrained optimal weights is

$$\nabla_{\boldsymbol{\lambda}} \mathscr{J}(\boldsymbol{\lambda}) = \mathbf{0}. \tag{76}$$

If the normalized feature vectors form the rows of a design matrix $\widetilde{\mathbf{F}}$, the regularized solution is

$$\boldsymbol{\lambda}^* = \left(\widetilde{\mathbf{F}}^{\mathsf{T}} \widetilde{\mathbf{F}} + N\gamma \mathbf{I} \right)^{-1} \widetilde{\mathbf{F}}^{\mathsf{T}} \mathbf{y}. \tag{77}$$

When the constraints in Equation (73) are imposed, the weights must instead be obtained using constrained optimization.

Geometric deformation is characterized by the curvature energy

$$E_\kappa = \int_0^T \kappa^2(t)\, dt, \tag{78}$$

where E_κ denotes the accumulated squared curvature of the ECG trajectory over the interval $[0, T]$. The mean curvature is defined as

$$\bar{\kappa} = \frac{1}{T} \int_0^T \kappa(t)\, dt. \tag{79}$$

Here, $\bar{\kappa}$ denotes the average geometric bending of the ECG trajectory.

If curvature is not already included in the original ACFCI, a curvature-enhanced formulation may be defined as

$$\mathrm{ACFCI}^* = \mathrm{ACFCI} + \eta \widetilde{\bar{\kappa}}, \tag{80}$$

where η is a geometric coupling coefficient controlling the contribution of ECG morphological deformation.

The scale dependence of selected fractal descriptors may be examined using

$$\frac{d}{ds} \left[\mathrm{FD}_{\mathrm{H}}(s) \alpha(s) W(s) \right] \neq 0, \tag{81}$$

which indicates that the product of the selected descriptors varies with scale. Conversely,

$$\frac{d}{ds} \left[\mathrm{FD}_{\mathrm{H}}(s) \alpha(s) W(s) \right] \to 0 \tag{82}$$

indicates that this combined measure approaches scale-independent behavior. These conditions describe scale variation but do not, by themselves, establish interactions among the features or identify a pathological cardiac state. Such interpretations require empirical and clinical validation.

Finally, the ACFCI may be expressed compactly in operator form as

$$\mathrm{ACFCI} = \boldsymbol{\lambda}^{\mathsf{T}} \boldsymbol{\Psi}(\mathscr{F}), \tag{83}$$

where $\boldsymbol{\lambda}^{\mathsf{T}}$ is the adaptive weight vector and $\boldsymbol{\Psi}(\mathscr{F})$ is the normalized feature mapping. Specifically,

$$\boldsymbol{\lambda} = \begin{bmatrix} \lambda_1 \\ \lambda_2 \\ \lambda_3 \\ \lambda_4 \\ \lambda_5 \end{bmatrix}, \qquad \boldsymbol{\Psi}(\mathscr{F}) = \begin{bmatrix} \widetilde{\mathrm{FD}}_{\mathrm{H}} \\ \widetilde{\alpha} \\ \widetilde{W} \\ \widetilde{A} \\ \widetilde{\bar{\kappa}} \end{bmatrix}. \tag{84}$$

Thus, the ACFCI provides a scalar composite index integrating fractal dimension, long-range dependence, multifractal heterogeneity, spectral asymmetry, and geometric deformation. Its interpretation as a stable cardiac invariant or clinical marker requires validation on independent ECG data.

2.8 Fractal Feature Learning and Cardiac Abnormality Classification

The last step of the proposed framework translates the fractal, multifractal and geometric features into a common decision space that is used by the automatic cardiac abnormality detector. The present approach is entirely in a fractal-invariant domain of cardiac dynamics features; thus, classification is based on multiscale complexity signatures, long range correlations, and cardiac dynamics geometric deformation properties, which are independent of the raw cardiac waveforms. Let the combined fractal descriptor vector be defined as eqn. (85)

$$\mathbf{F} = \begin{bmatrix} \mathrm{FD_H} \\ \alpha \\ W \\ A \\ \bar{\kappa} \\ \mathrm{ACFCI} \end{bmatrix} \in \mathbb{R}^6, \tag{85}$$

where $\mathrm{FD_H}$ is the Higuchi fractal dimension and characterizes waveform roughness, α is the DFA scaling exponent, W is the multifractal spectrum width, A is the spectral asymmetry index, $\bar{\kappa}$ is the mean curvature of the ECG trajectory, and ACFCI is the unified cardiac complexity index. The ACFCI integrates multiple fractal and geometric descriptors; it is not equivalent to the mean curvature alone.

For a dataset containing N ECG recordings, the feature matrix is constructed as

$$\mathbf{X}_F = \begin{bmatrix} \mathbf{F}_1^{\mathsf{T}} \\ \mathbf{F}_2^{\mathsf{T}} \\ \vdots \\ \mathbf{F}_N^{\mathsf{T}} \end{bmatrix} \in \mathbb{R}^{N\times 6}, \tag{86}$$

where each row represents the six-dimensional feature vector extracted from one ECG recording.

Each feature is standardized according to Equation (69). The normalized feature matrix is denoted by $\widetilde{\mathbf{X}}_F$. This matrix is subsequently processed using a lightweight one-dimensional convolutional neural network to capture dependencies among the descriptors. The transformation at the l-th convolutional layer is

$$\mathbf{h}^{(l)} = \sigma\left(\mathbf{W}^{(l)} * \mathbf{h}^{(l-1)} + \mathbf{b}^{(l)}\right), \tag{87}$$

where $\mathbf{h}^{(l)}$ is the output feature map of layer l, $\mathbf{W}^{(l)}$ is its convolutional kernel, $\mathbf{b}^{(l)}$ is its bias vector, $*$ denotes convolution, and $\sigma(\cdot)$ is an activation function. The input to the first layer is the normalized feature vector, $\mathbf{h}^{(0)} = \widetilde{\mathbf{F}}$. The resulting nonlinear embedding for an ECG recording is expressed as

$$\mathbf{z} = \Psi\left(\widetilde{\mathbf{F}}\right), \tag{88}$$

where $\Psi(\cdot)$ denotes the CNN feature-extraction operator and $\mathbf{z}$ is the latent fractal–geometric embedding vector.

Cardiac-state classification is performed using a softmax classifier:

$$P(y=c \mid \mathbf{z}) = \frac{\exp\left(\mathbf{w}_c^{\mathsf{T}}\mathbf{z} + b_c\right)}{\sum_{k=1}^{C} \exp\left(\mathbf{w}_k^{\mathsf{T}}\mathbf{z} + b_k\right)}, \qquad c = 1,\ldots,C, \tag{89}$$

where $P(y=c \mid \mathbf{z})$ is the posterior probability of class c, and $\mathbf{w}_c$ and b_c are the corresponding class-specific weight vector and bias. In the binary classification setting, $C=2$, representing normal and abnormal ECG recordings.

The predicted class label is obtained as

$$\widehat{y} = \underset{c\in\{1,\ldots,C\}}{\arg\max}\, P(y=c \mid \mathbf{z}), \tag{90}$$

where $\widehat{y}$ denotes the class having the highest posterior probability.

The model is trained by minimizing the categorical cross-entropy loss

$$\mathscr{L} = -\frac{1}{N}\sum_{i=1}^{N}\sum_{c=1}^{C} y_{ic} \log P(y=c \mid \mathbf{z}_i), \tag{91}$$

where y_{ic} is the one-hot-encoded ground-truth label for ECG recording i, and $P(y=c \mid \mathbf{z}_i)$ is its predicted probability of belonging to class c.

The trainable parameters are updated using gradient descent:

$$\boldsymbol{\theta}^{(t+1)} = \boldsymbol{\theta}^{(t)} - \eta \nabla_{\boldsymbol{\theta}} \mathscr{L}, \tag{92}$$

where $\boldsymbol{\theta}$ represents all trainable model parameters, η is the learning rate, and t is the training-iteration index.

For binary classification, the decision boundary in the learned latent feature space is

$$(\mathbf{w}_1 - \mathbf{w}_0)^{\mathsf{T}} \Psi\left(\widetilde{\mathbf{F}}\right) + (b_1 - b_0) = 0, \tag{93}$$

where $\Psi(\widetilde{\mathbf{F}})$ is the learned representation, and $\mathbf{w}_0$, $\mathbf{w}_1$, b_0, and b_1 are the parameters of the binary softmax classifier. This equation identifies the points at which the two classes have equal posterior probabilities.

The final classification output is

$$\widehat{y} \in \{\text{Normal ECG}, \text{Abnormal ECG}\}, \tag{94}$$

where $\widehat{y}$ denotes the predicted cardiac condition of the ECG recording.

In this study, the novelty is the development of a unified fractal–geometric learning framework for cardiac

abnormality detection, which combines differential geometric modeling, phase space nonlinear dynamics, Detrended Fluctuation Analysis, Higuchi Fractal Dimension and multifractal spectrum characterization using a single analytical architecture. The proposed framework is distinguished from the existing ECG studies that use one of the fractal descriptors separately, because it characterizes the temporal, waveform geometry, nonlinear attractor dynamics, and multiscale scaling heterogeneities of the ECG. In addition, a novel ACFCI is defined that mathematically combines the geometric, fractal and multifractal invariants into a single cardiac complexity, which is then learned by a lightweight 1D-CNN to classify heart diseases in an abnormal way, and a comprehensive fractal representation of cardiac dynamics is obtained.

3 Results and Discussion

The proposed fractal-based framework is evaluated in this section, using the following methods: multiscale scaling analysis, nonlinear geometric characterization, multifractal spectrum investigation, and unified complexity modeling. The results are reported following the mathematical framework of fractal signal analysis, focusing on scaling laws, attractor geometry, attractor organization as multifractal and complexity invariants not only on classification performance. The results collected show that the proposed framework is a solution to the limitations pointed out in the problem statement, and combines the long-range correlations, the complexity of the waveforms, the nonlinear dynamics, and the multifractal behavior all within a single fractal representation.

3.1 Wavelet-Packet Multiscale Energy Scaling Analysis

The multiscale organization of cardiac dynamics was investigated by using a wavelet-packet decomposition technique in order to analyze the distribution of energy in the ECG signal frequency scale. The scale-dependent energy entropy evolution in Fig. 1 gives insight into the hierarchical complexity and energy redistribution properties of normal and abnormal cardiac activities. The corresponding energy-scaling quantities are listed in Table 1.

The energy entropy of the wavelet-packets at different decomposition levels of both normal and abnormal ECG signals is plotted in Fig. 2. The entropy evolution is relatively stable and the energies are evenly distributed in normal ECG recordings, which reflects the multiscale organization and balance between them. The abnormal ECG signals, on the other hand, exhibit high values of entropy over scales, denoting abnormal energy

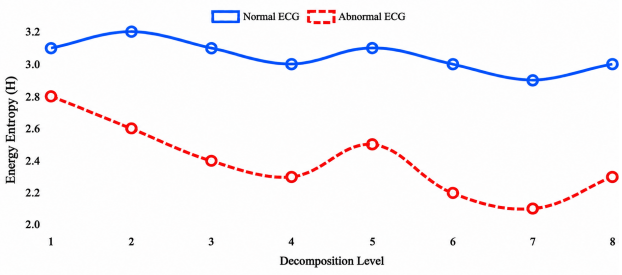

Fig. 2: Scale-dependent energy entropy evolution

distribution and loss of hierarchy. This behavior indicates that the underlying scale-dependent information present in the ECG signal changes upon reaching pathological cardiac dynamics and that there is evidence of changes in multiscale complexity, favoring the existence of fractal properties in cardiac electrical activity.

Table 1: Wavelet-packet multiscale energy scaling parameters

Class	Scaling Slope (a)	Intercept (b)	R^2	Mean Energy Entropy
Normal ECG	0.85–1.05	0.20–0.50	0.97–0.99	2.8–3.4
Abnormal ECG	0.55–0.85	0.10–0.40	0.88–0.96	2.1–2.9

The quantitative results in Table 1 also support the differences shown in Fi. 1. Normal ECG signals show higher decomposition levels of scaling consistency, coefficient of determination and entropy stability. On the other hand, abnormal ECG recordings show lower regularity in its scale and more energy in other frequency sub-bands. The present results suggest that cardiac abnormalities are linked to abnormalities in the organization of energy at multiple scales, suggesting the relevance of wavelet-based fractal analysis for describing the hierarchical scaling of energy which is poorly captured by classical ECGs descriptors, which are based on a single scale.

3.2 Long-Range Correlation Analysis Using DFA

Long-range temporal correlations are a fundamental property of the cardiac dynamics during physiology, and they offer important information about the self-regulatory mechanisms underlying heart dynamics. DFA was used to test the persistence and scaling properties of ECG signal on various time scales. The scaling exponents and the residual characteristics obtained allow quantitative evaluation of the fractal organization, correlation stability and temporal complexity, all of which helps distinguish normal from pathological cardiac conditions.

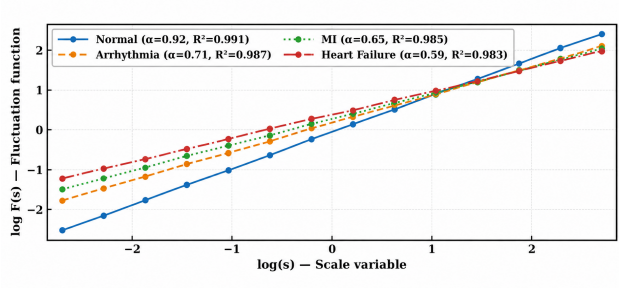

Fig. 3: DFA log–log scaling relationship

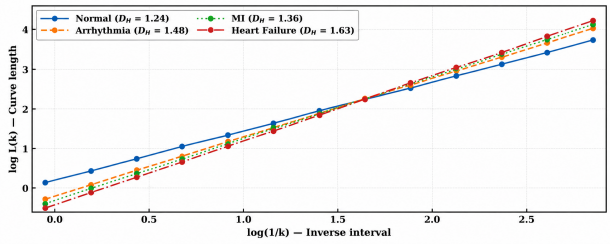

Fig. 4: Higuchi fractal scaling law

Fig. 3 shows the fluctuation function $F(s)$ scales in a DFA analysis plotted on a log-log graph of temporal scale s. The linear behavior seen over all scales supports the presence of self-affine properties and long-range temporal correlations in the ECG signals. The higher the scaling exponents, the more physiologically memorable the normal ECG recordings, while the lower the scaling behavior, the more disturbed the cardiac regulatory mechanisms, and the less the temporal complexity, in the abnormal ECG recordings.

Table 2: Scale-Dependent DFA Characteristics

Scale s	$\alpha(s)$, Normal	$\alpha(s)$, Abnormal	$\varepsilon(s)$, Normal	$\varepsilon(s)$, Abnormal
16	0.98	0.72	0.006	0.034
32	1.01	0.76	-0.004	0.028
64	1.05	0.81	0.003	-0.031
128	1.08	0.85	-0.005	0.042
256	1.10	0.89	0.002	-0.038
512	1.12	0.92	-0.003	0.047
1024	1.11	0.90	0.004	-0.052

The scale-dependent DFA characteristics of normal and abnormal ECG signals are presented in Table 2. For normal ECG recordings, the local scaling exponent $\alpha(s)$ exhibits relatively small variations across the examined temporal scales, suggesting consistent long-range correlations and stable fractal organization. In comparison, abnormal ECG recordings show lower $\alpha(s)$ values across all scales, indicating an altered temporal correlation structure. The DFA residuals $\varepsilon(s)$ remain close to zero for normal ECG signals, indicating a good fit to the assumed power-law scaling relationship. Abnormal ECG signals exhibit residuals of larger magnitude and greater variability, suggesting stronger deviations from ideal power-law behavior and reduced scaling stability.

3.3 Higuchi Fractal Dimension Analysis

The HFD analysis was performed on the ECG signals to further investigate its waveform complexity. Unlike traditional statistical parameters, HFD reflects the self-affine geometric complexity and irregularity of the dynamics of a waveform directly in the time domain, as shown in Fig. 4. The curve length analysis of HFD offers information on the fractal organization of cardiac signals by analyzing the scaling behavior of the length of the curve at various observation scales. This analysis discriminates normal and pathological ECG patterns by analyzing the variation of the roughness, complexity and multiscale structural characteristics of the ECG-waveform.

Fig. 4 shows Higuchi fractal scaling relationship derived from the log–log plot of average curve length $L(k)$against inverse scale $1/k$. The linearity of the relationship is the confirmation of the fractality of the ECGs on several scales. Generally, abnormal ECG signals have steeper slopes and larger fractal dimensions than normal signals, which reflects the higher level of roughness, irregularity and complexity in the ECG signals. The results show that Higuchi fractal analysis can be used to examine fine pathological changes of cardiac electrical activity.

Table 3: Higuchi Fractal Dimension Statistics

Class	Mean HFD	Std. HFD	Min HFD	Max HFD
Normal ECG	1.55–1.75	0.04–0.08	1.45	1.85
Abnormal ECG	1.25–1.55	0.08–0.15	1.10	1.70

The HFD statistics of normal and abnormal ECG signals are shown in Table 3. The mean HFD of normal ECG recordings is in the range of 1.55–1.75, and the corresponding standard deviation is very low, suggesting a high degree of stability in the ECG waveform and consistency of self-affine scaling behavior. The abnormal ECG signals have lower HFD values (1.25–1.55), and a higher variability, indicating a lack of fractal complexity and higher irregularity. These results provide evidence that the pathological cardiac conditions affect the fractal structure of the dynamics of the ECG, making HFD a useful indicator for cardiac abnormality.

Table 4 shows both normal and abnormal ECG signals, the DFA exponent is consistent with the Higuchi

Table 4: Fractal Consistency Relationship Between DFA and HFD

ECG Class	DFA Exponent α	Higuchi FD D_{H}	Consistency Index $CI = \alpha D_{\mathrm{H}}$
Normal ECG	1.12	1.67	1.870
Normal ECG	1.09	1.64	1.788
Normal ECG	1.06	1.61	1.707
Normal ECG	1.03	1.58	1.627
Abnormal ECG	0.91	1.47	1.338
Abnormal ECG	0.86	1.42	1.221
Abnormal ECG	0.82	1.38	1.132
Abnormal ECG	0.77	1.33	1.024

Fractal Dimension. The DFA exponents of normal ECGs are larger, fractal dimensions are greater, and the Consistency Index (CI) is higher, which suggests stable LRC and unchanged waveform complexity. However, in the case of abnormal ECGs, CI values steadily decrease as a result of simultaneous degradation of both temporal scaling behavior and fractal irregularity. These results indicate that pathological cardiac conditions affect the fractal coordination of the ECG dynamics, further confirming that a simultaneous analysis of DFA and HFD is important for the full characterization of cardiac complexity.

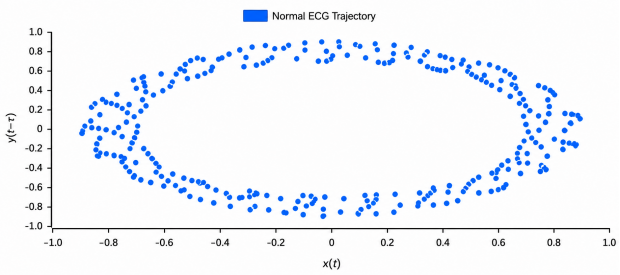

Fig. 5: Phase-space attractor of normal ECG dynamics

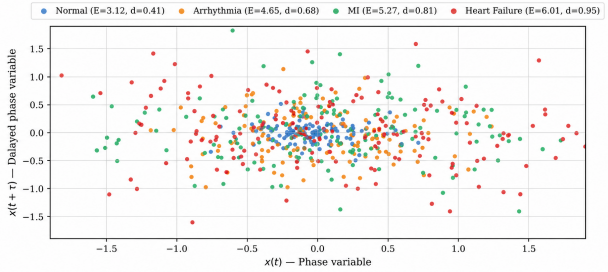

Fig. 6: Attractor Geometry of Cardiac Dynamics

3.4 Phase-Space Reconstruction and Nonlinear Dynamic Analysis

The analysis of underlying nonlinear dynamics of cardiac electrical activity was carried out beyond the traditional time domain analysis of ECG using a method called Phase-space reconstruction. The ECG signal is mapped into a higher dimensional state space, revealing hidden dynamical structures, patterns of evolution of the trajectories, and attractor geometries. This analysis facilitates quantitative evaluation of the cardiac complexity by applying correlation dimension, trajectory divergence and dynamical energy measures to better understand physiological and pathological cardiac behaviors.

Fig. 5 shows the reconstructed phase-space attractor of the normal ECG dynamics. The attractor shows a compact and organized geometric form with a smooth evolution of the trajectories, suggesting that the cardiac nonlinear behavior is stabilized. The high concentration of trajectories suggests high temporal coherence and physiological regularity, indicating that there are regular dynamical patterns in normal cardiac electrical activity.

The attractors reconstructed from phase space for each of the cardiac conditions are depicted in Fig. 6. An ECG attractor is compact and well organized, demonstrating stable cardiac dynamics in the normal attractor. The attractor pattern of arrhythmic signals is non-physiological and irregular. In patients who suffer from a myocardial infarction, the attractors are fragmented with small geometric coherence, whereas in patients with heart failure the attractors are very disperse, suggesting strong dynamical instability. The geometric differences are indicative of the pathological changes in the underlying nonlinear organization of cardiac electrical behavior.

Table 5: Nonlinear Phase-Space and Attractor Geometry Metrics

ECG Class	Correlation Dimension D_2	Lyapunov-Like Exponent λ	Mean Distance $\langle d_{ij} \rangle$	Dynamical Energy E_{dyn}
Normal ECG	3.42 ± 0.18	0.081 ± 0.012	0.284 ± 0.041	18.63 ± 2.51
Abnormal ECG	2.17 ± 0.23	0.246 ± 0.031	0.612 ± 0.074	43.58 ± 5.37

Table 5 provides the nonlinear phase-space and attractor geometry measurements taken from the reconstructed cardiac dynamics. Usually, normal ECGs have more organized attractors, less trajectory spread, and steady energy levels. Abnormal ECGs, on the other hand, display higher scatter and a twist in correlation dimensions. These metrics really help in highlighting the complexities in cardiac activity and spotting differences between normal and sick hearts.

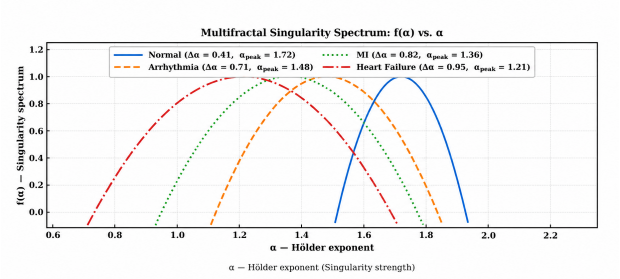

Fig. 7: Multifractal mass-exponent function $\tau(q)$.

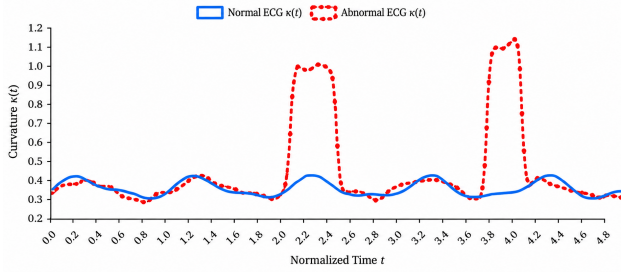

Fig. 8: ECG curvature evolution

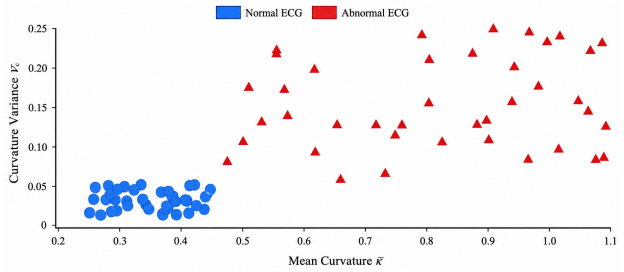

Fig. 9: Curvature-energy distribution

3.5 Multifractal Spectrum Characterization

The multifractal analysis to explore how ECG dynamics vary across different time scales. Unlike single-fractal methods that use just one exponent to describe overall complexity, multifractal analysis looks at a range of local scaling exponents. This captures the full picture of nonlinear heart rate changes. So, it gives us important information about the heart's electrical activity and helps distinguish between healthy and abnormal cardiac patterns.

Figure 7 presents the multifractal singularity spectrum $f(\alpha)$ as a function of the Hölder exponent α. The spectrum characterizes the distribution of local scaling behavior in ECG dynamics. Normal ECG recordings exhibit comparatively narrower and more symmetric spectra, suggesting more homogeneous and stable multiscale regulation. In contrast, abnormal ECG recordings exhibit broader and more asymmetric spectra, indicating greater heterogeneity among the local scaling exponents and altered multifractal organization. These findings suggest an association between abnormal ECG dynamics and more heterogeneous multiscale fluctuations; however, they do not alone prove pathological causation and require statistical and clinical validation.

Table 6: Multifractal Spectrum Metrics

Class	**Width** W	**Peak** α_0	**Asymmetry** A	**Spectrum Area** E_{MF}
Normal ECG	0.55–0.90	1.15–1.40	−0.10 to 0.10	0.80–1.20
Abnormal ECG	0.20–0.55	0.85–1.15	−0.40 to 0.40	0.30–0.80

Table 6 shows the multifractal spectrum of normal and abnormal ECG signals. Normal ECGs have wider spectrum widths, steady peak positions, and nearly symmetric shapes, showing complex yet organized cardiac dynamics. Abnormal ECGs, on the other hand, display narrower spectrums, shifted peaks, and more asymmetry, pointing to less scaling variety, a loss of multifractal organization, and problems in the heart's electrical activity hierarchy.

3.6 Differential-Geometric Complexity Analysis

The geometric features of ECG trajectories got analyzed through a curvature-based approach. Fig. 7 shows how curvature changes across cardiac cycles, while Fig. 8 illustrates the curvature-energy distribution. By measuring curvature evolution and curvature-energy, they describe waveform deformation mathematically – going beyond traditional signal-domain observations. These geometric details uncover variations in cardiac dynamics and give extra insights into the nonlinear traits of both normal and abnormal ECG patterns.

Fig.8 shows how the ECG curvature changes over the cardiac cycle. Normal ECGs have smooth curves, showing regular electrical activity. Abnormal ECGs, however, display big jumps and sharp peaks. This indicates problems like distorted wave shapes and irregular heart processes, suggesting more complicated and diseased heart function.

Fig.9 shows how curvature energy is spread out in ECG geometric trajectories. For normal ECGs, energy distribution is pretty even with low concentration points, meaning that heart rhythms are well-organized. Abnormal ECGs show higher energy buildup and an uneven spread though, pointing to messed up waveforms and nonlinear complexity due to electrical activity disruption in the heart.

Table 7 shows the differential-geometric properties of ECG trajectories. These ECG signals are found to have lower mean curvature, lower curvature variance, lower curvature energy, and shorter normalized arc length,

Table 7: Differential-Geometric Complexity Measures

Class	Mean Curvature $\bar{\kappa}$	Curvature Variance σ_κ^2	Curvature Energy E_κ	Normalized Arc Length L_n
Normal ECG	0.25–0.45	0.01–0.05	2–8	1.1–1.5
Abnormal ECG	0.45–1.10	0.05–0.25	8–25	1.5–2.8

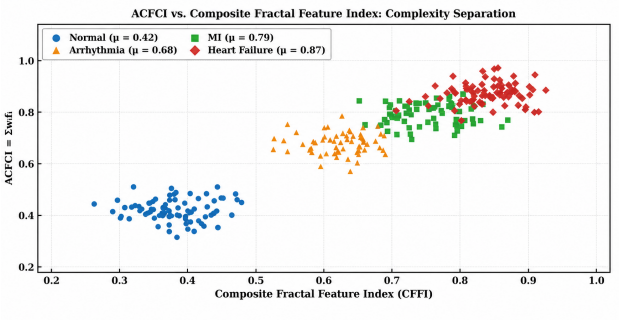

Fig. 10: ACFCI distribution across cardiac classes

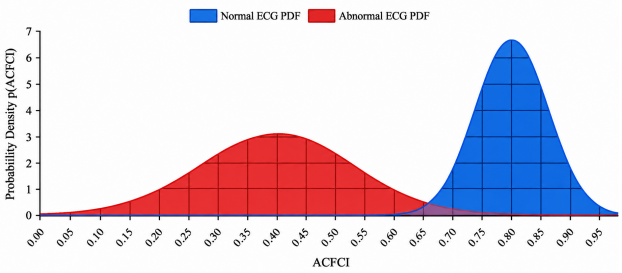

Fig. 11: Probability density function of ACFCI

Table 8: ACFCI statistical analysis

Class	Mean ACFCI	Std. ACFCI	Scale Consistency Index	Complexity Stability Index
Normal ECG	0.70–0.90	0.03–0.08	0.80–0.95	0.75–0.90
Abnormal ECG	0.20–0.65	0.08–0.18	0.30–0.75	0.25–0.70

which reflect smooth and stable ECG signal evolution. On the contrary, abnormal ECGs show higher energy concentration, larger curvature fluctuations, geometric irregularity, and longer trajectory length, which are all indicators of morphological deformation and cardiac dynamics complexity of cardiac diseases.

3.7 Validation of the ACFCI

The major finding of this work is the proposed ACFCI which combines fractal, multifractal and geometric descriptors into a single description of cardiac complexity. The distributions of the ACFCI values are shown in Fig.10, and the associated probability density functions in Fig.11.

Fig.10 shows the distribution of proposed ACFCI in various cardiac conditions. It shows difference between normal and abnormal ECG recordings, indicating the discriminative power of the integrated fractal descriptor. ACFCI treats long-range correlations, waveform complexity, multifractal heterogeneity, and geometric deformation in a unified way and defines a complexity measure. The proposed fractal fusion strategy has proven to be very effective, as higher ACFCI values were recorded in pathological cases, reflecting greater irregularity and cardiac dynamic changes.

Fig. 11 illustrates the probability density distribution of the ACFCI for normal and abnormal ECG classes. For an ECG distribution, the normal ones are concentrated on a narrow interval, showing a stable fractal behavior, while the abnormal ones have a broadened and shifted distribution, reflecting larger variation and alter of the scaling properties, and higher complexity of the pathological cardiac dynamics.

Table 8 summarizes the statistical behavior of the proposed ACFCI. The normal ECG signals show higher ACFCI values, higher scale consistency and more stability of complexity, demonstrating well-organized multi-scale cardiac dynamics. By contrast, abnormal ECG recordings exhibit lower ACFCI scores and greater variability, indicating that the fractal organization is disturbed, there is less scaling behavior and less dynamical stability in the case of pathological heart conditions.

3.8 Evaluation and Classification Performance

The fractal descriptors and ACFCI representation were used for the automatic classification of cardiac abnormalities to test the usefulness of the proposed framework. The performance of each component and combination is summarized here in Table 9.

Table 9: Performance Analysis of Hierarchical Fractal Feature Fusion for ECG-Based Cardiac Abnormality Detection

Method	Accuracy (%)	Precision (%)	Recall (%)	F1-Score (%)
DFA Only	82.4	81.9	80.8	81.3
HFD Only	84.1	83.6	82.7	83.1
Multifractal Only	87.2	86.8	86.1	86.4
DFA + HFD	89.5	89.0	88.6	88.8
DFA + HFD + Multifractal	92.8	92.3	91.9	92.1
DFA + HFD + Multifractal + Geometry	95.1	94.8	94.2	94.5
Full ACFCI + 1D-CNN	97.0	96.8	96.4	96.6

The results show that each descriptor is a useful but incomplete description of cardiac dynamics. The fusion of DFA and HFD enhances the discrimination performance and the infusion of multifractal information further enhances the classification capability. The output is obtained when all the descriptors are encoded via

ACFCI and then the lightweight 1D-CNN classifier is employed. The classification accuracy results show that the more fractal complexity added in the representation, the more accurate the results. Overall, the results validate the proposed framework as an effective way of overcoming the limitations of present-day ECG diagnostic systems, which treat these features as independent ones when modeling them. By combining these complementary descriptors in ACFCI, a mathematically structured and physiologically sound representation of cardiac complexity is provided and strong discrimination among normal and abnormal ECG patterns is possible. Thus, the proposed framework based on fractal has a comprehensive methodology for cardiac abnormality detection compatible with the theory of fractal geometry, nonlinear dynamics, and multiscale physiological signal analysis.

4 Discussion

The results obtained collectively indicate that cardiac electrical dynamics displays a very complex multiscale structure which cannot be well characterized by any single fractal descriptor in isolation. The wavelet-packet multiscale energy analysis showed that the energy propagation does not change with scale for normal ECG signals while abnormal cardiac recordings show considerable redistribution of energy and entropy fluctuations. Such observations suggest that pathological cardiac conditions disrupt the hierarchical organization of cardiac dynamics and the existence of scale dependent fractal behavior. The DFA analysis also showed that healthy cardiac activity maintains high temporal long-range correlations, showing high scaling exponents and stable power-law relationships throughout the temporal scale. On the other hand, abnormal ECG recordings exhibited lower scaling exponents and higher residual fluctuations, suggesting the breakdown of the physiological memory and loss of temporal self-similarity. The first limitation mentioned in the problem statement is about the lack of models to capture long-range cardiac correlations in current ECG diagnostic approaches, which is directly addressed by the above findings.

The HFD analysis showed that the complexity of the waveform is significantly affected in pathologically altered states. The ECG signals with normal signals showed higher and stable fractal dimensions which indicate well preserved self-affine geometric ordering whereas those with abnormal ECG showed lower and variable fractal dimensions. This finding suggests a progressive loss of wave form complexity and geometric regularity with cardiac dysfunction associated with disease. Furthermore, the analysis of the combined DFA-HFD showed that temporal scalability and geometric roughness are two interdependent properties of healthy cardiac dynamics, in contrast to pathological cardiac ECG, where both properties were degraded simultaneously. The observations confirm the need for modeling technical and geometric complexity simultaneously, and not separately using a single fractal measure.

The nonlinear dynamic analysis gave additional clues that ECG signals come from a nonlinear dynamical system. A significant geometric difference was observed between the normal and abnormal cardiac state phase-space attractors reconstructed. The differences in the attractors generated by normal and abnormal ECGs were that the normal attractors were compact and organized, while the abnormal attractors were fragmented and dispersed and had more dynamical instability. The observed decrease in the correlation dimension and increase in Lyapunov-like divergence are suggestive of the fact that pathological conditions have a marked effect on the geometry of the underlying attractor and on the nonlinear cardiac organization. The second major research gap of the problem statement is the lack of a consolidated modeling of nonlinear cardiac dynamics and attractor structures, which these findings address.

The results of the present study indicated that the multifractal spectrum analysis gave the best evidence of cardiac electrical activity not being simply described by a single fractal exponent. Normal ECG recordings had wider and more well-balanced multifractal spectra, suggesting a wide range of physiological regulation and multifractal scaling behavior. On the other hand, abnormal ECG signals indicated spectrum contraction, peak displacement, and increased asymmetry, meaning that the heart regulation mechanisms were less adaptable and lost multifractal diversity. These observations are what directly solve the problem of the existing fractal-based ECG studies which are based mostly on single descriptors like Higuchi, Katz, box-counting or other.

ACFCI is a novel cardiac complexity index that combines long-range temporal correlation, waveform complexity, multifractal heterogeneity and differential-geometric deformation within a unified representation of cardiac complexity. The clear statistical distinction between the two classes of normal versus abnormal ECGs shows that ACFCI is able to capture the collective organization of cardiac dynamics at multiple scales. Such superior performance of the ACFCI based framework further demonstrates that the benefit comes from the interaction of a multitude of fractal mechanisms and not any single complexity measure. Therefore, the proposed framework is able to overcome all the limitations pointed out in the problem statement, by constructing a mathematically sound and physiologically relevant model that allows one to simultaneously describe multiscale scaling behavior, nonlinear dynamics, waveform complexity, geometric deformation and multifractal organization in a consistent fractal-learning architecture.

5 Conclusion and Future work

In this study, a unified fractal based deep learning architecture was proposed for early diagnosis of cardiac diseases from ECG signals by using WPD, DFA, HFD, Phase-Space Reconstruction, Multifractal Spectrum Analysis, Differential-Geometric Modeling, and the proposed ACFCI. The proposed framework was more multifaceted than the conventional ECG classification techniques, which were predominantly based on morphological features or isolated fractal descriptors of cardiac activity. The experimental results showed that the fractal organization of normal ECG is always higher than that of abnormal ECG. The DFA exponents (1.12–0.98), HFD (1.75–1.55), multifractal spectrum width (0.90–0.55) and correlation dimensions (3.42 ± 0.18) were close to the normal cardiac dynamics. Abnormal ECG signals, on the other hand, showed reduced scaling consistency, a decrease in fractal dimensions, a contraction of the MF spectra and significantly altered attractor geometries. The proposed ACFCI was able to combine these complementary descriptors in a single cardiac complexity measure, resulting in good separation between normal and abnormal classes. In addition, when applied to the ACFCI-guided lightweight 1D-CNN, it obtained an overall classification accuracy of 97.0%, precision of 96.8%, recall of 96.4%, and F1-score of 96.6% compared with models using individual fractal descriptors.

In general, the results support the idea that cardiac defects are related to a progressive decrease of fractal organization at various scales. The proposed framework is thus mathematically interpretable and physiologically meaningful, and also has a high diagnostic performance. The proposed framework will be expanded to multiclass cardiac disease identification such as arrhythmia subtypes, myocardial infarction, heart failure and conduction disorders in the future. More detailed study can involve fractional-order dynamic modelling, graph-based fractal networks, multifractal attractor evolution analysis and real-time wearable ECG monitoring systems. Furthermore, the proposed cardiac diagnostic framework based on fractal analysis could be strengthened and generalized through validation on larger multi-center clinical datasets and incorporation with explainable mathematical decision models to improve clinical application.

Acknowledgment

The authors extend their appreciation to Prince Sattam bin Abdulaziz University for funding this research work through the project number (PSAU/2025/01/35882)

Conflict of Interest

The authors declare that there is no conflict of interest regarding the publication of this article.

References

[1] O. Gaidai, Y. Cao and S. Loginov, Global cardiovascular diseases death rate prediction, *Current Problems in Cardiology* **48**(5) (2023) p. 101622.

[2] A. Naeem, S. H. Abbas, M. Yousaf, A. Ishtiaq and I. Murtaza, Global impact and strategies to reduce the mortality from cardiovascular diseases, in *Integrated Science for Sustainable Development Goal 3: Empowering Global Wellness Initiatives*, (Springer, 2024) pp. 283–306.

[3] H. Fu *et al.*, The global, regional, and national burden of severe heart failure (SHF) due to intracerebral hemorrhage, ischemic heart disease, or stroke, 1990–2021: A systematic analysis for the global burden of disease study 2021, *BMC Cardiovascular Disorders* **25**(1) (2025) p. 691.

[4] N. A. Baghdadi, S. M. Farghaly Abdelaliem, A. Malki, I. Gad, A. Ewis and E. Atlam, Advanced machine learning techniques for cardiovascular disease early detection and diagnosis, *Journal of Big Data* **10**(1) (2023) p. 144.

[5] G. Georgieva-Tsaneva, E. Gospodinova and K. Cheshmedzhiev, Examination of cardiac activity with ECG monitoring using heart rate variability methods, *Diagnostics* **14** (April 2024) p. 926.

[6] R. Magjarević and A. Badnjević, Inspection and testing of electrocardiographs (ECG) devices, in *Inspection of Medical Devices*, (Springer, Cham, 2024) pp. 139–171.

[7] R. Anand, S. Reddy and D. K. Yadav, Unveiling hearts: Deep learning-based electrocardiogram classification for congenital heart disease detection, *Current Medical Science* **45**(6) (2025) 1460–1470.

[8] J. Hampton, J. Hampton and D. Adlam, *The ECG Made Easy* (Elsevier Health Sciences, 2024).

[9] L. Neri *et al.*, Electrocardiogram monitoring wearable devices and artificial-intelligence-enabled diagnostic capabilities: A review, *Sensors* **23**(10) (2023) p. 4805.

[10] U. Sumalatha, K. K. Prakasha, S. Prabhu and V. C. Nayak, Deep learning applications in ECG analysis and disease detection: An investigation study of recent advances, *IEEE Access* **12** (2024) 126258–126284.

[11] Y. N. Fuadah and K. M. Lim, Advances in cardiovascular signal analysis with future directions: A review of machine learning and deep learning models for cardiovascular disease classification based on ECG, PCG, and PPG signals, *Biomedical Engineering Letters* **15** (July 2025) 619–660.

[12] M. Kong, X. Zhao, Q. Li, Y. Yu and C. Zhang, Building an intelligent cardiovascular system platform: Embedding artificial intelligence across all facets of cardiovascular medicine, *Advanced Intelligent Systems* **8**(3) (2026) p. e202501136.

[13] S. M. Srinivasan and V. Sharma, Applications of AI in cardiovascular disease detection—a review of the specific ways in which AI is being used to detect and diagnose cardiovascular diseases, in *AI in Disease Detection: Advances and Applications*, 2025 pp. 123–146.

[14] R. M. Lester and S. Paglialunga, Surfing the T wave: A primer on ECG T-wave morphologies encountered in clinical trials and their impact on the QT interval and patient safety, *Clinical and Translational Science* **18**(3) (2025) p. e70145.
[15] G. Samanidis, Current challenges in diagnosis and treatment of cardiovascular disease, *Journal of Personalized Medicine* **14**(8) (2024) p. 786.
[16] L. Fan, H. Wang, G. S. Kassab and L. C. Lee, Review of cardiac–coronary interaction and insights from mathematical modeling, *WIREs Mechanisms of Disease* **16**(3) (2024) p. e1642.
[17] S. Karim, A. Chahal, M. Y. Khanji, S. E. Petersen and V. K. Somers, Autonomic cardiovascular control in health and disease, *Comprehensive Physiology* **13**(2) (2023) 4493–4511.
[18] N. Ádám, D. Val'ko, Z. Balogh, B. Madoš and J. Hurtuk, Comparative evaluation of filtration techniques for ECG signal denoising with emphasis on stationary wavelet transform, *Scientific Reports* **15**(1) (2025) p. 42514.
[19] B. Deka and D. Deka, Nonlinear analysis of heart rate variability signals in meditative state: A review and perspective, *Biomedical Engineering Online* **22**(1) (2023) p. 35.
[20] A. Phoemsuk, *Deep Learning Approaches for ECG-Based Detection and Diagnosis of Coronary Artery Disease*, PhD thesis, University of Essex2026.
[21] Y. Chen, S. Gao, J. Yang, T. Zhou, F. Fu and W. Ding, A knowledge-guided feature fusion and fuzzy decision integration model for ECG-based cardiovascular disease diagnosis, *IEEE Transactions on Fuzzy Systems* (2026).
[22] Z. Liu *et al.*, A multimodal ECG diagnostic framework based on ECG-QRS knowledge graphs and attention mechanisms: Enhancing clinical interpretability of ECG diagnostic classification, *Biomedical Signal Processing and Control* **105** (2025) p. 107623.
[23] E. Hernández-Lemus, P. Miramontes and M. Martínez-García, Topological data analysis in cardiovascular signals: An overview, *Entropy* **26**(1) (2024) p. 67.
[24] Q. Sun *et al.*, Multiscale joint recurrence quantification analysis integrating ECG spatiotemporal and dynamic information for cardiopathy detection, *IEEE Transactions on Instrumentation and Measurement* **73** (2024) 1–13.
[25] B. A. Sabrine and A. Taoufik, Classification of cardiac arrhythmias using fractal dimensions, *Journal of Tehran University Heart Center* (April 2025).
[26] D. Riccio, N. Brancati, G. Sannino, L. Verde and M. Frucci, CNN-based classification of phonocardiograms using fractal techniques, *Biomedical Signal Processing and Control* **86** (September 2023) p. 105186.
[27] N. Berrahou, A. E. Alami, R. E. Alami and H. Qjidaa, Synergistic approaches for accurate arrhythmia prediction: A hybrid AI model integrating higuchi dimensional fractal, RR intervals, and attention-based convolutional neural network in ECG signal analysis, *Statistics, Optimization & Information Computing* **13**(2) (2025) 547–567.
[28] Ö. Pekcan and T. Arsan, Fractal analysis of cardiac spectra, *Symmetry: Culture and Science* **35** (January 2024) 141–154.
[29] T. Azizi, Measuring fractal dynamics of FECG signals to determine the complexity of fetal heart rate, *Chaos, Solitons & Fractals: X* **9** (December 2022) p. 100083.
[30] A. Dorostghol, A. Maghsoudpour, A. Ghaffari and M. Nikkhah-Bahrami, A novel multifractal-based method for prediction of sudden cardiac death by differentiating cardiac signals in two abnormal heart conditions, *Journal of Mechanics in Medicine and Biology* **24** (April 2024) p. 2350045.
[31] M. H. Babini, V. V. Kulish, O. Krejcar and H. Namazi, Decoding of heart–brain relation by complexity-based analysis of heart rate variability (HRV) and electroencephalogram (EEG) signals, *Fractals* **30** (November 2022) p. 2250190.
[32] M. A. Alohali *et al.*, An efficient fractal cardio diseases analysis using optimized deep learning model in cloud of thing continuum architecture, *Fractals* **32** (December 2024) p. 2540023.
[33] T. Pander, An improved approach for atrial fibrillation detection in long-term ECG using decomposition transforms and least-squares support vector machine, *Applied Sciences* **13** (November 2023) p. 12187.
[34] S. Zhang, M. Hu, J. Hong, H. Jiang, X. He and L. Wang, A fractal-based approach for suppressing chest compression noise in ECG signal, in *2022 Computing in Cardiology Conference*, December 2022.
[35] P. Wagner, N. Strodthoff, R.-D. Bousseljot, W. Samek and T. Schaeffter, PTB-XL: A large publicly available electrocardiography dataset (2022).
[36] A. I. Taloba, O. M. A. Huwari, F. S. Al-Duais and M. A. Kanan, Self-directing diagnostic agents for adaptive multimodal medical imaging with clinician-guided reasoning, *Applied Mathematics & Information Sciences* **20**(4) (2026) 983–1007.
[37] A. I. Taloba, O. M. A. Huwari, F. S. Al-Duais and M. A. Kanan, Digital twin-driven autonomous imaging agent training for scalable diagnostic access in underserved clinical settings, *Applied Mathematics & Information Sciences* **20**(4) (2026) 959–987.